Save 50% with the IET Summer Sale

Use code SUMMER23 to save on over 650+ selected engineering and technology books.

*Discount only available on selected print books between 21 August to 15 September

The Institution of Engineering and Technology

Browse the sale titles

IET Communications

Research Article

IET Journals
The Institution of Engineering and Technology

Digital linear GFSK demodulator for IoT devices

ISSN 1751-8628
Received on 12th June 2017
Revised 18th April 2018
Accepted on 25th May 2018
E-First on 7th September 2018
doi: 10.1049/iet-com.2018.5040
www.ietdl.org

Rodrigo Aldana-Lopez[1], Jose Valencia-Velasco[2] ✉, Omar Longoria-Gandara[2], Luis Pizano-Escalante[2]

[1]*Intel GDC, Av. del Bosque 1001, Zapopan, Jal. 45019, Mexico*

[2]*Department of Electronics, Systems and IT, ITESO, Periferico Sur Manuel Gomez Morin 8585, Tlaquepaque, Jal. 45604, Mexico*

✉ *E-mail: ng100357@iteso.mx*

Abstract: Companies and developers of emerging Internet-of-Things (IoT) technologies consider Bluetooth low-energy (BLE) standard as a strong candidate to be the backbone of wireless IoT devices and support their low-power requirements. Likewise, the BLE has adopted Gaussian frequency shift-keying (GFSK) signalling due to its power and spectral efficiencies, which are the most fundamental performance criteria for modulation schemes. For this reason, it is worthwhile to research and develop transceivers that maintain these advantages and achieve a low-complexity implementation for the digital modulator and demodulator. Different techniques have been proposed for this purpose, such as hardware usage optimisation, efficient pulse shaping and decomposition of the signal. This study presents a novel linear GFSK demodulator which has the following attractive advantages: low complexity, near-optimal performance in the additive white Gaussian noise channel and the possibility of operating with different GFSK modulators (with a nominal modulation index of 0.5) so it could be applied in BLE devices. In addition, the theoretical error probability is obtained and compared with simulation results.

1 Introduction

Communications systems can be classified in terms of four kinds of efficiencies: radio spectrum utilisation (bandwidth efficiency), bit-error rate (BER) efficiency (noise immunity), power efficiency (link budget, selection of the amplifiers and the number of antennas) and cost efficiency (low hardware and software resources in transmitters and receivers). The design of wireless communication systems implies a trade-off between these four categories, the environment and the use case required, i.e. telemetry in aerospace applications, telephony or Internet-of-Things (IoT) applications. In this context, the selection of a specific digital modulation technique mainly impacts the spectrum utilisation and the cost parameters. Continuous phase modulation (CPM) [1] is a class of digital modulation that includes frequency-shift keying (FSK) and phase-shift keying (PSK) techniques with a signal phase constrained to be continuous as is described in detail in [2].

Continuous phase FSK (CPFSK) is a CPM subclass oriented to bandwidth conservation (spectral efficiency) with constant-envelope and memory due to its continuous phase. According to the pulse shape and the modulation index of the baseband digital signal used in CPFSK, it is possible to have different schemes such as minimum shift keying (MSK), Gaussian MSK (GMSK) and Gaussian FSK (GFSK) with rectangular and Gaussian pulse shaping.

The efficiency of CPM techniques has been confirmed by industrial communications standards. For instance, Bluetooth uses GFSK [3] due to its constant envelope property and less stringent linearity requirement on the power amplifier, making it a popular modulation scheme for low-power and low-cost applications such as IoT [4].

Due to CPM detection complexity problems as described in [5], two different approaches can be considered to reduce the complexity of the implementations. The first one focuses on the optimisation of hardware resources at the modulator [6–8]. In relation to low complexity demodulators, the authors of [4, 9, 10] propose low complex GFSK demodulators based on zero-crossing detector.

Another approach oriented to reducing the complexity of the communication system is based on the representation of the CPM signals using PAM (pulse amplitude modulation) decomposition. Laurent shows in [11] that any CPM signal can be decomposed into a finite number of PAM pulses; as a result, the signal can be reconstructed with good accuracy by one main pulse. This has several advantages in the design of modulators and demodulators that have been reported in the literature [12–15]. There are other approximations for CPM signals; e.g. Brown and Vigneron [16] propose a basis function expansion with Legendre polynomials and B-splines, and Liang *et al.* [17] present an alternative linear approximation of GMSK signals to LD [11], by using a discrete representation.

In this paper, a novel linear GFSK demodulator is proposed. It obtains an estimation of the transmitted symbols based on the linear data model detailed in [17]. The proposed demodulator has the following attractive features: (i) because of its linearity, it has a simple structure with low complexity; (ii) the performance is very close to the near-optimal Viterbi receiver in the additive white Gaussian noise (AWGN) channel model; and (iii) its structure allows it to operate with both the 'exact' (direct generation of GFSK signals) and linear modulators [17]. The proposal is hereafter called linear GFSK demodulator based on pseudo-inverse estimation (LPIE).

The paper proceeds as follows: The GFSK system model is described in detail in Section 2. Section 3 presents two implementations of the proposed demodulator (LPIE), while the theoretical performances in terms of error probability are obtained in Sections 4 and 5, respectively. The optimal parameters of the design and the computational complexity are provided in Section 6. Simulation results are analysed and compared with the theoretical performance in Section 7. Finally, conclusions are drawn in Section 8.

2 GFSK system model

The purpose of the communication system is to transmit a set of symbols $s_n \in \{+1, -1\}$ from one side of the system to the other. The first part of the system is a differential encoder as shown in Fig. 1. This type of encoding takes an input string of symbols $\{s_0, s_1, \ldots, s_n\}$ $s_n \in \{+1, -1\}$ and converts it into a new string of symbols $\{z_0, z_1, \ldots, z_n\}$ following the rule given by

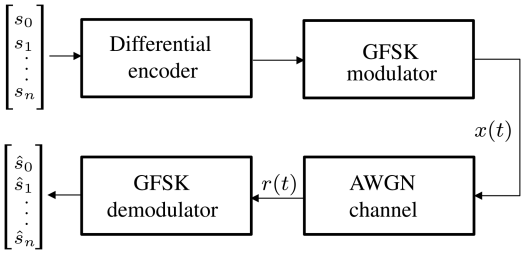

Fig. 1 *General block diagram of a communication system with GFSK modulation where data is deferentially encoded and phase modulated*

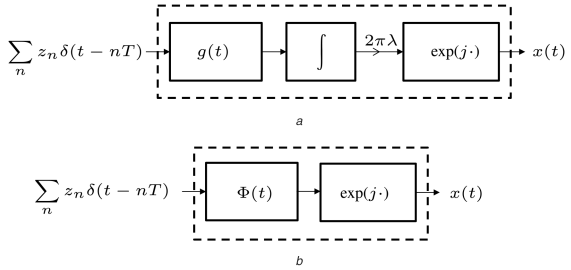

Fig. 2 *Baseband model for two different approaches to GFSK modulators with*
(a) *g*(*t*) pulse shaping, where *δ*(*t*) stands for the Dirac delta, ***(b)*** Φ(*t*) pulse shaping

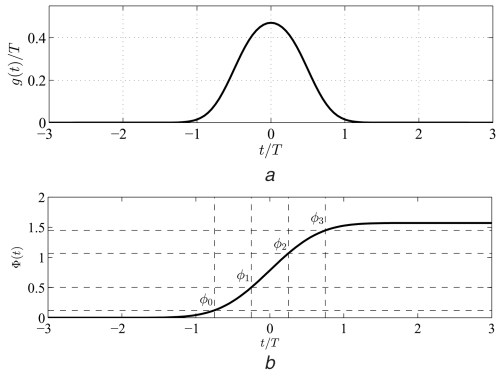

Fig. 3 *Signals of GFSK modulation process*
(a) Pulse *g*(*t*) with *BT* = 0.5, ***(b)*** Pulse Φ(*t*)

$$z_n = \begin{cases} s_n s_{n-1}, & n > 0 \\ s_0, & n = 0 \end{cases}. \tag{1}$$

The modulator uses the scheme represented in Fig. 2*a*. This type of modulation takes the input symbols z_n and generates a pulse train $p(t)$ defined as

$$p(t) = \sum_n z_n g(t - nT) \tag{2}$$

where $n \in \mathbb{Z}$, T denotes the symbol-time duration and $g(t)$ is the pulse shaping based on a Gaussian function shown in Fig. 3*a* and described as

$$g(t) = \frac{1}{2T}\left[Q\left(2\pi BT\left(\frac{t - T/2}{\sqrt{\ln(2)}T}\right)\right) - Q\left(2\pi BT\left(\frac{t + T/2}{\sqrt{\ln(2)}T}\right)\right)\right] \tag{3}$$

where B is the -3 dB bandwidth, BT is the bandwidth–time product and $Q(t)$ is the Q-function defined as

$$Q(t) = \frac{1}{\sqrt{2\pi}}\int_t^\infty \exp(-\tau^2/2)\mathrm{d}\tau\,. \tag{4}$$

The signal $p(t)$ in (2) is integrated and used to modulate a complex exponential, generating what is called the baseband form of the frequency modulation

$$x(t) = \exp\left(j2\pi\lambda\int_{-\infty}^t p(\tau)\mathrm{d}\tau\right) = \exp(j\varphi(t)) \tag{5}$$

in which λ represents the modulation index and

$$\varphi(t) = 2\pi\lambda\int_{-\infty}^t p(\tau)\mathrm{d}\tau \tag{6}$$

represents the phase signal. The modulation index is defined as

$$\lambda = 2T\Delta f\,. \tag{7}$$

For example, in BLE the nominal value of λ is 0.5, so with this value, the maximum frequency deviation is $\Delta f = 1/4T$. Also in BLE, $BT = 0.5$ and the duration of $g(t)$ is approximately 3 T as shown in Fig. 2*a*; this is known as the partial response CPM [18].

Another interesting implementation for generating $x(t)$ is based on [17] and it can be obtained as follows. Let a function be defined as

$$\Phi(t) = 2\pi\lambda\int_{-\infty}^t g(\tau)\mathrm{d}\tau, \tag{8}$$

such that the phase impulse response acquires the new form given by

$$\begin{aligned}\varphi(t) &= 2\pi\lambda\sum_n z_n\int_{-\infty}^t g(\tau - nT)\mathrm{d}\tau \\ &= \sum_n z_n\Phi(t - nT)\,.\end{aligned} \tag{9}$$

This scheme is shown in Fig. 2*b* and is equivalent to the previous scheme [17]. Another representation of the modulator presented in [17] considers two consecutive samples per symbol period of $x(t)$ as follows:

$$\begin{aligned}x(kT + T_\mathrm{d}) &= \exp\left(j\sum_n z_n\Phi((k-n)T + T_\mathrm{d})\right) \\ x(kT + T_\mathrm{d} + T/2) &= \exp\left(j\sum_n z_n\Phi((k-n)T + T/2 + T_\mathrm{d})\right)\end{aligned} \tag{10}$$

where $k \in \mathbb{Z}$ and T_d represents a time deviation in the range $[0, T/2]$. Then by expanding the expressions in (10) and neglecting the smaller terms, the following linear version is obtained:

$$\begin{bmatrix}\hat{x}_k \\ \hat{x}_{k+\frac{1}{2}}\end{bmatrix} = j^k\boldsymbol{A}\begin{bmatrix}s_{k+1} \\ s_k \\ s_{k-1}\end{bmatrix} \tag{11}$$

with

$$\begin{aligned}\hat{x}_k &= \hat{x}(kT + T_\mathrm{d}) \\ \hat{x}_{k+\frac{1}{2}} &= \hat{x}(kT + T/2 + T_\mathrm{d})\end{aligned} \tag{12}$$

and

$$\boldsymbol{A} = \begin{bmatrix}-\sin\phi_0\sin\phi_2 & j\cos\phi_0\sin\phi_2 & \cos\phi_0\cos\phi_2 \\ -\sin\phi_1\sin\phi_3 & j\cos\phi_1\sin\phi_3 & \cos\phi_1\cos\phi_3\end{bmatrix} \tag{13}$$

where

$$\begin{aligned}\phi_0 &= \Phi(-T + T_{\mathrm{d}})\\ \phi_1 &= \Phi(-T/2 + T_{\mathrm{d}})\\ \phi_2 &= \Phi(T_{\mathrm{d}})\\ \phi_3 &= \Phi(T/2 + T_{\mathrm{d}})\,.\end{aligned} \tag{14}$$

as shown in Fig. 3*b*. Expression (11) constitutes the linear GFSK modulator, with $\lambda = 0.5$, proposed in [17] with a memory length of three symbol periods. Hence, this modulator belongs to the family of CPM with partial response as described in [19].

Using any of these representations of the transmitted GFSK baseband signal, the signal received under the AWGN channel is given by

$$r(t) = x(t) + \eta(t) \tag{15}$$

where $\eta(t)$ is a zero-mean additive complex white Gaussian noise with variance $\sigma^2 = N_0/2$ per real and imaginary components and power spectral density of $N_0/2$.

3 Linear GFSK demodulator based on pseudo-inverse estimation

3.1 Motivation

Taking as a reference (11), which represents the linear GFSK modulator, a receiver is designed to obtain an estimate of the transmitted symbols. Since there are more variables than equations, the linear GFSK modulator is composed of an undetermined system of equations when solving for s_{k+1}, s_k and s_{k-1}. Assuming $r(t) = x(t)$ then a linear GFSK demodulator consists of solving this system of equations. With the notation $\boldsymbol{x} = [\hat{x}_k, \hat{x}_{k+\frac{1}{2}}]^{\mathrm{T}}$ and $\boldsymbol{s} = [s_{k+1}, s_k, s_{k-1}]^{\mathrm{T}}$ where $[\,\cdot\,]^{\mathrm{T}}$ denotes transpose, expression (11) can be rewritten as

$$\boldsymbol{x} = j^k \boldsymbol{A}\boldsymbol{s}\,. \tag{16}$$

There will be an exact solution of (16) only if $\boldsymbol{x} \in R(j^k\boldsymbol{A})$ where $R(\,\cdot\,)$ denotes the range of a matrix as is presented in [20]. It could be the case in which this problem has no exact solution, particularly when the received signal in the presence of noise is used. Fortunately, there are many approaches to this problem and one well-established solution is the *least-squares method*, i.e. choose an approximate solution $\tilde{\boldsymbol{s}}$ such that the residual error

$$\| \boldsymbol{x} - j^k\boldsymbol{A}\tilde{\boldsymbol{s}} \|^2$$

is minimised. It is shown in [20] that

$$\tilde{\boldsymbol{s}} = (j^k\boldsymbol{A})^{\dagger}\boldsymbol{x}$$

minimises the residual error, where $(\,\cdot\,)^{\dagger}$ denotes the Moore–Penrose pseudo-inverse matrix.

Motivated by this result, a demodulator is proposed with the following structure:

$$\begin{bmatrix}\hat{s}_{k+1}\\ \hat{s}_k\\ \hat{s}_{k-1}\end{bmatrix} = (j^k\boldsymbol{A})^{\dagger}\begin{bmatrix}r_k\\ r_{k+\frac{1}{2}}\end{bmatrix} \tag{17}$$

with

$$\begin{aligned}r_k &= r(kT + T_{\mathrm{d}})\\ r_{k+\frac{1}{2}} &= r(kT + T/2 + T_{\mathrm{d}})\,.\end{aligned} \tag{18}$$

and $\hat{s}_{k+1}, \hat{s}_k$ and $\hat{s}_{k-1}$ being the symbol estimates at the receiver. Under this perspective, the demodulator is a linear GFSK based on pseudo-inverse estimation.

Due to the fact that one symbol-time duration of the modulated signal contains information about 3 symbols, the proposed demodulator uses the Moore-Penrose pseudo-inverse to obtain an estimate of each one of these three transmitted symbols. Therefore, by taking a linear combination of these three estimates (taken at three different symbol-times), one combined estimated symbol can be expressed as

$$\hat{s}_k = h_1\hat{s}_k^{(1)} + h_2\hat{s}_k^{(2)} + h_3\hat{s}_k^{(3)} = \sum_{m=1}^{3} h_m\hat{s}_k^{(m)} \tag{19}$$

where $h_m \in \mathbb{R}$ are the linear combination coefficients that can be optimised to have a better symbol estimate. The superscript 1 refers to the estimate of s_k obtained from the previous symbol-time duration; likewise, the superscripts 2 and 3 refer to the estimates of s_k obtained from the current and the subsequent symbol-time durations, respectively.

3.2 Proposal 1: demodulation scheme LPIE-2S

Taking two samples in a symbol-time duration of the received signal, and with the superscript notation described in (19), an estimate of the transmitted symbols can be obtained as follows:

$$\begin{bmatrix}\hat{s}_{k+1}^{(1)}\\ \hat{s}_k^{(2)}\\ \hat{s}_{k-1}^{(3)}\end{bmatrix} = (j^k\boldsymbol{A})^{\dagger}\begin{bmatrix}r_k\\ r_{k+\frac{1}{2}}\end{bmatrix}. \tag{20}$$

A weighted estimate of s_k can be derived from (20) with the following expression:

$$h_2\hat{s}_k^{(2)} = [0 \quad h_2 \quad 0](j^k\boldsymbol{A})^{\dagger}\begin{bmatrix}r_k\\ r_{k+\frac{1}{2}}\end{bmatrix}. \tag{21}$$

Making the change $k \to k-1$ in (20) in order to see the demodulator in the previous symbol-time duration results in a second estimate for s_k

$$h_1\hat{s}_k^{(1)} = [h_1 \quad 0 \quad 0](j^{k-1}\boldsymbol{A})^{\dagger}\begin{bmatrix}r_{k-1}\\ r_{k-\frac{1}{2}}\end{bmatrix}. \tag{22}$$

Also with $k \to k+1$ for the demodulator, a symbol-time duration after the current one results in the third estimate for s_k

$$h_3\hat{s}_k^{(3)} = [0 \quad 0 \quad h_3](j^{k+1}\boldsymbol{A})^{\dagger}\begin{bmatrix}r_{k+1}\\ r_{k+\frac{3}{2}}\end{bmatrix}. \tag{23}$$

In this way, from (19) and (21)–(23), the estimated symbol $\hat{s}_k$ can be written as a linear combination of the samples $[r_{k-1}, r_{k-\frac{1}{2}}, \ldots, r_{k+\frac{3}{2}}]$ as follows:

$$\hat{s}_k = [W_1 \quad W_2 \quad \ldots \quad W_6]\begin{bmatrix}r_{k-1}\\ r_{k-\frac{1}{2}}\\ \vdots\\ r_{k+\frac{3}{2}}\end{bmatrix}. \tag{24}$$

From (22) and with $\boldsymbol{\Lambda} = \boldsymbol{A}^{\dagger}$, the coefficient $W_1 \in \mathbb{C}$ can be calculated as

$$W_1 = h_1[1 \quad 0 \quad 0]\frac{1}{j^{k-1}}\boldsymbol{\Lambda}\begin{bmatrix}1\\ 0\end{bmatrix} = \frac{h_1}{j^{k-1}}\Lambda_{11}\,. \tag{25}$$

In a similar way, the remaining coefficients, $W_i \in \mathbb{C}$, can be calculated as

$$
\begin{aligned}
W_2 &= \frac{h_1}{j^{k-1}}\Lambda_{12} \\
W_3 &= \frac{h_2}{j^{k}}\Lambda_{21} \\
W_4 &= \frac{h_2}{j^{k}}\Lambda_{22} \\
W_5 &= \frac{h_3}{j^{k+1}}\Lambda_{31} \\
W_6 &= \frac{h_3}{j^{k+1}}\Lambda_{32}\,.
\end{aligned} \tag{26}
$$

It is important to note that the coefficients W_i are computed offline since the matrix $\boldsymbol{A}$ is known a priori at the transmitter and the receiver.

3.3 Proposal 2: demodulation scheme LPIE-1S

Due to the fact that the LPIE-2S demodulation scheme requires two samples per symbol-time duration, the following implementation of LPIE, hereafter named LPIE-1S, consists of taking one sample per symbol-time duration. Four estimates associated with one symbol are obtained. Hence, the resulting symbol estimate is given by

$$
\hat{s}_k = \sum_{m=1}^{4} h_m \hat{s}_k^{(m)} \tag{27}
$$

where the superscript 1 refers to the estimate of s_k obtained two symbol-time durations ago; likewise the supper-indices 2, 3 and 4 refer to the estimates of s_k obtained from the previous, the current and the subsequent symbol-time durations, respectively.

From (11), two consecutive samples are

$$
\hat{x}_k = j^k(A_{11}s_{k+1} + A_{12}s_k + A_{13}s_{k-1}) \tag{28}
$$

$$
\hat{x}_{k+1} = j^{k+1}(A_{11}s_{k+2} + A_{12}s_{k+1} + A_{13}s_k)\,. \tag{29}
$$

Both (28) and (29) can be written as

$$
\begin{bmatrix} \hat{x}_k \\ \hat{x}_{k+1} \end{bmatrix} = j^k \boldsymbol{B} \begin{bmatrix} s_{k+2} \\ s_{k+1} \\ s_k \\ s_{k-1} \end{bmatrix} \tag{30}
$$

with

$$
\boldsymbol{B} = \begin{bmatrix} 0 & A_{11} & A_{12} & A_{13} \\ jA_{11} & jA_{12} & jA_{13} & 0 \end{bmatrix}. \tag{31}
$$

Thus, four received symbols can be estimated from (30). Likewise, the structure of the demodulator is given by

$$
\begin{bmatrix} \hat{s}_{k+2}^{(1)} \\ \hat{s}_{k+1}^{(2)} \\ \hat{s}_k^{(3)} \\ \hat{s}_{k-1}^{(4)} \end{bmatrix} = (j^k \boldsymbol{B})^{\dagger} \begin{bmatrix} r_k \\ r_{k+1} \end{bmatrix} \tag{32}
$$

and the weighted estimates for this demodulator are written as (see (33)) resulting in a symbol estimate expressed as

$$
\hat{s}_k = [W_1 \quad W_2 \quad \cdots \quad W_5] \begin{bmatrix} r_{k-2} \\ r_{k-1} \\ \vdots \\ r_{k+2} \end{bmatrix} \tag{34}
$$

Defining $\boldsymbol{\beta} = \boldsymbol{B}^{\dagger}$, the coefficients $W_i \in \mathbb{C}$ can be calculated as

$$
\begin{aligned}
W_1 &= \frac{h_1}{j^{k-2}}\beta_{11} \\
W_2 &= \frac{h_1}{j^{k-2}}\beta_{12} + \frac{h_2}{j^{k-1}}\beta_{21} \\
W_3 &= \frac{h_2}{j^{k-1}}\beta_{22} + \frac{h_3}{j^{k}}\beta_{31} \\
W_4 &= \frac{h_3}{j^{k}}\beta_{32} + \frac{h_4}{j^{k+1}}\beta_{41} \\
W_5 &= \frac{h_4}{j^{k+1}}\beta_{42}\,.
\end{aligned} \tag{35}
$$

Due to the imperfections of the demodulation, the output of these two proposals is complex in general, so the output of the demodulators can be described by the following real random variable:

$$
\Gamma = \Re\{\hat{s}_k\} \tag{36}
$$

where $\Re\{\cdot\}$ is the real component of $\{\cdot\}$.

4 Error probability for LPIE-2S

In this section, the error probability will be calculated when the transmitted signal is in the presence of AWGN. Based on the demodulation scheme proposed in (20) for LPIE-2S and considering (36), the probability of error is defined as

$$
\begin{aligned}
P_e = {} & P(\{\Gamma > 0\} \cap A_0) \\
& + P(\{\Gamma < 0\} \cap A_1)
\end{aligned} \tag{37}
$$

where $A_0 = \{s_k = -1\}$ and $A_1 = \{s_k = 1\}$. The definition in (37) describes the probability that: a binary symbol, $s_k = -1$, is transmitted and the received and decoded symbol, $\hat{s}_k = 1$, is received or a binary symbol, $s_k = 1$, is transmitted and the received and decoded symbol, $\hat{s}_k = -1$, is received. Therefore, (37) can be rewritten as

$$
\begin{aligned}
P_e = {} & P(\Gamma > 0 | A_0)P(A_0) \\
& + P(\Gamma < 0 | A_1)P(A_1)\,.
\end{aligned} \tag{38}
$$

$$
\begin{aligned}
h_1\hat{s}_k^{(1)} &= [h_1 \quad 0 \quad 0 \quad 0](j^{k-2}\boldsymbol{B})^{\dagger} \begin{bmatrix} r_{k-2} \\ r_{k-1} \end{bmatrix} \\
h_2\hat{s}_k^{(2)} &= [0 \quad h_2 \quad 0 \quad 0](j^{k-1}\boldsymbol{B})^{\dagger} \begin{bmatrix} r_{k-1} \\ r_k \end{bmatrix} \\
h_3\hat{s}_k^{(3)} &= [0 \quad 0 \quad h_3 \quad 0](j^{k}\boldsymbol{B})^{\dagger} \begin{bmatrix} r_k \\ r_{k+1} \end{bmatrix} \\
h_4\hat{s}_k^{(4)} &= [0 \quad 0 \quad 0 \quad h_4](j^{k+1}\boldsymbol{B})^{\dagger} \begin{bmatrix} r_{k+1} \\ r_{k+2} \end{bmatrix}
\end{aligned} \tag{33}
$$

Since s_k is a discrete random variable with uniform probability distribution over the set $\{-1, 1\}$, then

$$P(A_0) = P(A_1) = \frac{1}{2}. \tag{39}$$

It can be demonstrated that

$$P(\Gamma > 0 | A_0) = P(\Gamma < 0 | A_1) \tag{40}$$

so using (39) and (40), (38) can be simplified to

$$P_e = P(\Gamma < 0 | A_1). \tag{41}$$

Using the conditional probability of Γ defined as

$$P(\Gamma \in B | A_i) = \int_B f_{\Gamma|A_i}(\gamma) d\gamma \tag{42}$$

where $f_{\Gamma|A_i}(\gamma)$ is the conditional probability density function (PDF), B is any subset of the real numbers and A_i represents the binary events previously described, the probability of error is

$$P_e = \int_{-\infty}^{0} f_{\Gamma|A_1}(\gamma) d\gamma. \tag{43}$$

Since the demodulator is a linear system, for analysis purposes (43) can be calculated by first obtaining $f_{\Gamma|A_1}(\gamma)$ and considering the communication system without noise so that $x(t) = r(t)$, and then combining the result with the filtered noise.

4.1 PDF of the demodulated signal without noise

Taking as a reference [17] the transmitted signal can be expressed as

$$\begin{aligned} x_k &= \exp(j s_{k+1} s_k \theta_0 + j s_k s_{k-1} \theta_2) j^k s_{k-1}, \\ x_{k+\frac{1}{2}} &= \exp(j s_{k+1} s_k \theta_1 + j s_k s_{k-1} \theta_3) j^k s_{k-1}. \end{aligned} \tag{44}$$

Assuming $s_k = 1$, which corresponds to the event A_1, then the discrete random variable x_k takes values from a finite set of the complex numbers given by the combinations of the possible outcomes of s_{k-1} and s_{k+1}, i.e. s_{k-1} and s_{k+1} can only take two values; this implies that x_k can only take four values in (44). Therefore, the conditional PDF of x_k can be expressed as

$$f_{X_k|A_1}(x) = \frac{1}{4} \sum_{m=1}^{4} \delta(x - x_k^{(m)}) \tag{45}$$

where $\delta(x)$ is the Dirac delta and $x_k^{(m)}$ stands for the value of x_k using the mth combination of the random variables s_{k-1} and s_{k+1}.

Let γ_k be defined as Γ in the k-th symbol-time duration without noise. Using the output of the linear demodulator described in (24) and incorporated in (36), it can be observed that γ_k depends on $x_{k-1}, x_{k-\frac{1}{2}}, x_k, x_{k+\frac{1}{2}}, x_{k+1}$ and $x_{k+\frac{3}{2}}$. Computing each one of these samples with (44), it becomes evident that all together depend on the random variables $s_{k-2}, s_{k-1}, s_{k+1}$ and s_{k+2}, assuming s_k is known. With all these premises, γ_k is a discrete random variable that can take a value in a discrete set of the real numbers with 2^4 possible outcomes (i.e. it is a function of four independent random variables that take only two values).

Knowing all the possible outcomes, the PDF of γ_k is written as

$$f_{\gamma_k|A_1}(\gamma) = \frac{1}{M} \sum_{m=1}^{M} \delta(\gamma - \gamma_k^{(m)}) \tag{46}$$

where $M = 16$ and $\gamma_k^{(m)}$ is the mth possible outcome of γ_k.

4.2 PDF of the filtered noise

Considering the case with only noise at the input of the demodulator, it can be noticed from (24) that the output is a linear combination of six independent and identically distributed (i.i.d.) circularly-symmetric complex normal random variables, where the real and imaginary parts have a PDF of

$$f_{\mathcal{N}}(\eta) = \frac{1}{\sqrt{2\pi}\sigma} \exp\left(-\frac{\eta^2}{2\sigma^2}\right) \tag{47}$$

with a mean of zero and a variance of σ^2.

It is known that a linear combination of Gaussian random variables is also a Gaussian random variable. If the six samples of the noise are labelled as η_i for $i \in \{1, 2, \ldots, 6\}$, then the output of the demodulator ξ, i.e. the filtered noise, is

$$\xi = \Re\left\{\sum_{i=1}^{6} W_i \eta_i\right\} \tag{48}$$

where W_i stands for the coefficients of the filter that describes the demodulator in (24).

The variance of ξ can be obtained as

$$\begin{aligned} \mathrm{var}(\xi) &= \mathrm{var}\left(\Re\left\{\sum_{i=1}^{6} W_i \eta_i\right\}\right) \\ &= \sum_{i=1}^{6} \mathrm{var}(\Re\{W_i \eta_i\}) \\ &= \sum_{i=1}^{6} \mathrm{var}(\Re\{W_i\}\Re\{\eta_i\} - \Im\{W_i\}\Im\{\eta_i\}) \\ &= \sum_{i=1}^{6} \Re\{W_i\}^2 \mathrm{var}(\Re\{\eta_i\}) + \Im\{W_i\}^2 \mathrm{var}(\Im\{\eta_i\}) \\ &= \sum_{i=1}^{6} |W_i|^2 \sigma^2 = \sigma^2 G^2 \end{aligned} \tag{49}$$

where

$$G^2 = \sum_{i=1}^{6} |W_i|^2 \tag{50}$$

and $\Im\{\cdot\}$ is the imaginary component of $\{\cdot\}$. Then ξ has a PDF expressed as

$$f_{\Xi}(\xi) = \frac{1}{\sqrt{2\pi}\sigma G} \exp\left(-\frac{\xi^2}{2\sigma^2 G^2}\right). \tag{51}$$

4.3 PDF of the demodulated signal in the AWGN channel

Using the results from Sections 4.1 and 4.2 and knowing that the PDF of the sum of two independent random variables is the convolution of their PDF's, then

$$f_{\Gamma|A_1}(\gamma) = f_{\gamma_k|A_1}(\gamma) * f_{\Xi}(\gamma) \tag{52}$$

Substituting (46) and (51) into (52) leads to

$$f_{\Gamma|A_1}(\gamma) = \left(\frac{1}{M} \sum_{m=1}^{M} \delta(\gamma - \gamma_k^{(m)})\right) * \left(\frac{1}{\sqrt{2\pi}\sigma G} \exp\left(-\frac{\gamma^2}{2\sigma^2 G^2}\right)\right). \tag{53}$$

Using the property

$$\delta(x - a) * f(x) = f(x - a) \tag{54}$$

then (53) results in

$$f_{\Gamma|A_1}(\gamma) = \frac{1}{M\sqrt{2\pi}\sigma G}\sum_{m=1}^{M}\exp\left(-\frac{\left(\gamma-\gamma_k^{(m)}\right)^2}{2\sigma^2G^2}\right). \tag{55}$$

Substituting (55) into (43) the error probability is

$$P_{\mathrm{e}} = \frac{1}{M\sqrt{2\pi}\sigma G}\sum_{m=1}^{M}\int_{-\infty}^{0}\exp\left(-\frac{\left(\gamma-\gamma_k^{(m)}\right)^2}{2\sigma^2G^2}\right)\mathrm{d}\gamma. \tag{56}$$

It can be shown that

$$\int_{-\infty}^{0}\exp\left(-\frac{(x-a)^2}{b}\right)\mathrm{d}x = \frac{\sqrt{\pi b}}{2}\mathrm{erfc}\left(\frac{a}{\sqrt{b}}\right) \tag{57}$$

where

$$\mathrm{erfc}(x) = \frac{2}{\sqrt{\pi}}\int_{x}^{\infty}\exp\left(-u^2\right)\mathrm{d}u. \tag{58}$$

Then applying (57) into (56) leads to

$$P_{\mathrm{e}} = \frac{1}{2M}\sum_{m=1}^{M}\mathrm{erfc}\left(\frac{\gamma_k^{(m)}}{\sqrt{2}\sigma G}\right). \tag{59}$$

The signal-to-noise ratio (SNR) is related to σ by

$$\mathrm{SNR} = 10\log_{10}\left(Tf_{\mathrm{s}}\frac{P_x}{\sigma^2}\right) \tag{60}$$

where T is the symbol period, f_{s} is the sampling frequency and P_x is the power of the modulated signal calculated as

$$\begin{aligned} P_x &= \lim_{\rho\to\infty}\frac{1}{\rho}\int_{-\rho/2}^{\rho/2}|x(t)|^2\mathrm{d}t \\ &= \lim_{\rho\to\infty}\frac{1}{\rho}\int_{-\rho/2}^{\rho/2}|\exp(j\phi(t))|^2\mathrm{d}t = 1. \end{aligned} \tag{61}$$

Then using $Tf_{\mathrm{s}} = 2$

$$\sigma^2 = 2\cdot 10^{-\frac{\mathrm{SNR}}{10}}. \tag{62}$$

5 Error probability for LPIE-1S

In order to determine the error probability of the demodulator LPIE-1S, it can be observed from the expressions of the estimated symbols in (24) and (34) that all of them are linear combinations of the received samples weighted by the W_i coefficients previously calculated in Sections 3.2 and 3.3. Given this fact, (59) can be used for obtaining the error probability of LPIE-1S considering the following arguments:

The value of G is obtained by

$$G^2 = \sum_{i=1}^{5}|W_i|^2 \tag{63}$$

where W_i belongs to the LPIE-1S demodulator.

The parameter M in (46) can be calculated taking into account the fact that the output of the demodulation filter depends on $x_{k-2}, x_{k-1}, \ldots, x_{k+2}$ and thus on the six transmitted symbols $s_{k-3}, s_{k-2}, s_{k-1}, s_{k+1}, s_{k+2}$ and s_{k+3}. Therefore, γ_k has $M = 2^6$ possible outcomes labelled as $\gamma_k^{(m)}$.

In addition, $Tf_{\mathrm{s}} = 1$ because this demodulator uses one sample per symbol. Hence, the relation between σ and the SNR is

$$\sigma^2 = 10^{-\frac{\mathrm{SNR}}{10}}. \tag{64}$$

6 Optimal parameters and computational complexity for LPIE

Due to LPIE performance depends on the value of h_m coefficients, this section describes how they can be chosen by taking into account the error probability function with the goal of achieving the best performance of the proposed demodulator.

Let $\boldsymbol{h} = (h_1, h_2, h_3) \in \mathbb{R}^3$ for LPIE-2S and $\boldsymbol{h} = (h_1, h_2, h_3, h_4) \in \mathbb{R}^4$ for 1S. Then the probability error at a certain SNR can be viewed as a function of $\boldsymbol{h}$.

The function $P_{\mathrm{e}}(\boldsymbol{h})$ is indeterminate at $\boldsymbol{h} = \boldsymbol{0}$ because it would imply that $\hat{s}_k = 0$, so it is impossible to determine which symbol it represents. It can also be observed that the same value of error probability is achieved for $\boldsymbol{h}_0$ and $\ell\boldsymbol{h}_0\ \forall\ell > 0$, because both points differ only by a positive scalar that does not alter the detection of $\hat{s}_k$.

Therefore, the lines $\boldsymbol{h} = \ell\boldsymbol{h}_0$ with $\ell \in (0, \infty)$ are level hypersurfaces of $P_{\mathrm{e}}(\boldsymbol{h})$. This last statement implies that every proposed value for $\boldsymbol{h} \neq \boldsymbol{0}$ can be normalised, so the only relevant place to look for possible values of $\boldsymbol{h}$ is on the unit hyper-sphere $\|\boldsymbol{h}\| = 1$, where $\|\boldsymbol{h}\|$ denotes the Euclidean norm of $\boldsymbol{h}$. The contour map of $P_{\mathrm{e}}(\boldsymbol{h})$ for LPIE-2S considering SNR = 7 dB and maintaining $h_3 = 0$ is shown in Fig. 4. It can be observed how $P_{\mathrm{e}}(\boldsymbol{h})$ stays constant when moving along radial lines from the origin, since they correspond to level hypersurfaces of $P_{\mathrm{e}}(\boldsymbol{h})$. The projection on the plane of the unit sphere $\|\boldsymbol{h}\| = 1$ is shown in a dotted line, showing that restricting the search space to this surface does not alter the result.

In order to propose a set of possible values of $\boldsymbol{h}$, a minimisation of $P_{\mathrm{e}}(\boldsymbol{h})$ at a different SNR was solved (at least locally). The problem is stated as follows:

$$\begin{aligned} &\min P_{\mathrm{e}}(\boldsymbol{h}), \\ &\text{s.t. } \|\boldsymbol{h}\| = 1. \end{aligned} \tag{65}$$

A set of solutions to the problem in (65) for different values of SNR are shown in Fig. 5. These values were obtained using the interior point algorithm [21] with a function tolerance of 10^{-12} and a constraint tolerance of 10^{-6}. It is important to note that these solutions do not intend to guarantee global optimality of (65). The optimisation algorithm was executed for different SNR values to observe how the solutions for $\boldsymbol{h}$ change in different conditions. From Figs. 5*a* and *b*, it can be observed that the numerical solutions for $\boldsymbol{h}$, which the numerical solver delivered, remained at the same point, for practical purposes, over all tested SNR values, and the dominant coefficient is h_2 for LPIE-2S.

Table 1 shows the mean values of $\boldsymbol{h}$ for all tested SNR values (from 0 to 12 dB). These values will be used in the next section. Moreover, since the optimal parameter $\boldsymbol{h}$, the matrices $\boldsymbol{A}$, $\boldsymbol{\Lambda}$ and the weight W_i are calculated off-line, the complexity of computing every symbol estimate in (24) and (34) is shown in Table 2.

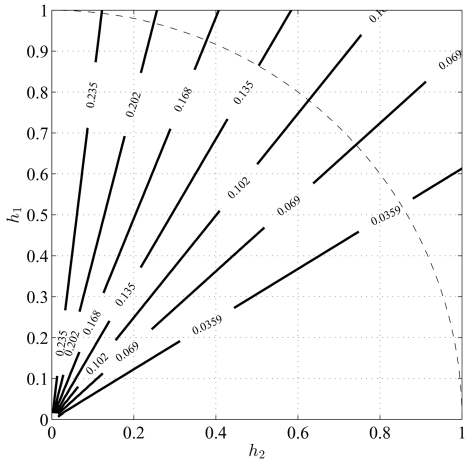

Fig. 4 *Contour map of $P_e(\boldsymbol{h})$ for LPIE-2S at SNR = 7 dB with $h_3 = 0$*

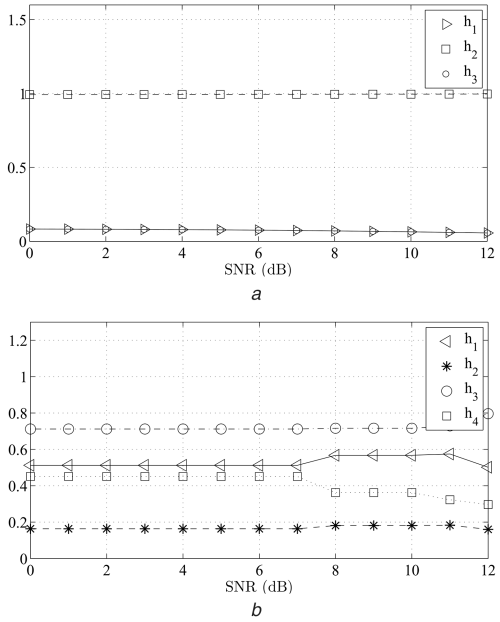

Fig. 5 *Values of* $\boldsymbol{h}$ *obtained from solving (65) at different values of SNR for LPIE*

(a) Numerical solutions of (65) for LPIE-2S and different values of SNR, ***(b)*** Numerical solutions of (65) for LPIE-1S and different values of SNR

Table 1 Values of $\boldsymbol{h}$ for the two proposed demodulators

	h_1	h_2	h_3	h_4
LPIE-2S	0.0731	0.9946	0.0731	n/a
LPIE-1S	0.5293	0.1689	0.7209	0.4090

Table 2 Computational complexity of LPIE

	Multiplications	Additions
LPIE-2S	6	5
LPIE-1S	5	4

7 Simulation results

This section presents simulation results of the LPIE demodulator taking BER performance as the figure-of-merit. The simulation scenario uses any of the baseband modulators described in Fig. 2, and the linear modulator of Section 2. Likewise, the demodulators employed were the LPIE and the Viterbi algorithm for GFSK signalling with a modulation index of 0.5. Frames with 10^6 binary symbols were injected into the modulator, computing the BER until 100 frames were processed or 10^3 errors were detected for each value of SNR; this allows the BER values to be statistically representative. Furthermore, the error probability of binary PSK (BPSK) digital modulation is used as a lower boundary.

An AWGN channel with a mean of zero is considered. Its variance is computed using (62) and (64) for the LPIE-2S and LPIE-1S, respectively. SNR values between 0 and 9 dB are considered.

The modulators were configured with the following parameters: $BT = 0.5$, a pulse $g(t)$ with $L = 3$ symbol periods, and a bit rate R_b of 10^6 bps [22]. The LPIE was configured taking into account a time deviation of $T_d = 0.25\,T$, $BT = 0.5$, and the elements of $\boldsymbol{h}$, computed off-line (before execution) by minimising the error probability, were taken from Table 1. The GFSK Viterbi parameters considered were: pulse length of three symbol periods, $BT = 0.5$ and a traceback of 20 symbol periods.

Figure 6 considers the exact modulator (direct generation of GFSK signals) and shows the simulated and error probability (obtained in Sections 4 and 5) of the LPIE-2S and LPIE-1S. In addition, the BER performance of the GFSK Viterbi and the error probability of the BPSK are included. It can be seen that the performance of all the proposed demodulators meets the specification for the BLE standard (BER of 0.1% at SNR of 21 dB) considering $\lambda = 0.5$. Furthermore, it can be observed that the LPIE-1S performs better than the LPIE-2S, maintaining an advantage of 0.3 dB. Unlike the Viterbi modulator that maintains a nearly-constant distance from BPSK, LPIE implementations are closer to BPSK at low SNR values and separate from BPSK as the SNR increases.

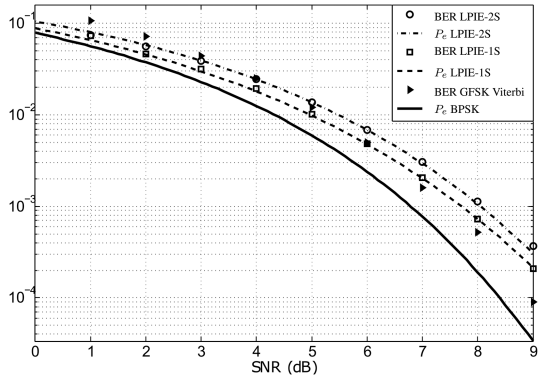

Fig. 6 *BER performance comparison between the LPIE-2S, the LPIE-1S (theoretical and simulated), the BPSK and the optimal Viterbi demodulator*

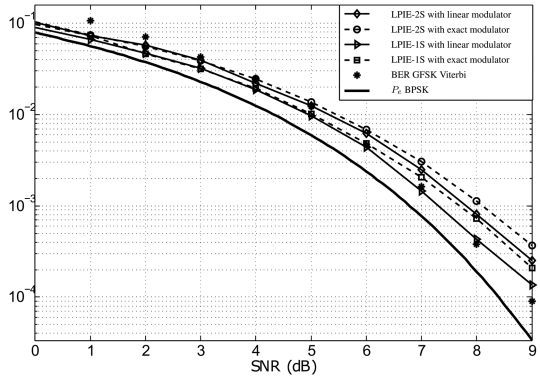

Fig. 7 *BER performance comparison between the LPIE-2S and the LPIE-1S using linear and exact modulators at the transmitter*

Fig. 7 shows the BER performance of the linear modulator [17] (revised in Section 2) and the exact one using the LPIE-2S and LPIE-1S at the receiver. It can be observed that the LPIE has a similar performance when it works with both modulators, and in this sense, it is a robust demodulator.

8 Conclusion

This paper proposes a novel linear GFSK demodulator for partial response signalling that can be used in Bluetooth low-energy for IoT wireless communications devices. This proposal has the following attractive features: its linear structure and robustness allow for operation with both exact and linear modulators achieving near-optimal performance in the AWGN channel. A complete description and detailed analysis of a linear GFSK modulator with a modulation index of 0.5 is revised. Consequently, the design and the structure of the proposed linear GFSK demodulator, LPIE, are derived. In addition, the theoretical error probability analysis is provided for two different implementations of LPIE for the AWGN channel. Finally, a method for selecting the demodulator parameters was developed based on the minimisation of error probability as a figure-of-merit.

Simulation results corroborate that the LPIE achieves a near-optimal performance in the AWGN channel, when it is compared with the GFSK Viterbi demodulator. Likewise, theoretical formulas for error probability, presented in Sections 4 and 5, match the simulation results. Furthermore, the results confirm that the LPIE is a demodulator that supports different types of GFSK modulator schemes at the transmitter.

9 References

[1] Sundberg, C.E.: 'Continuous phase modulation', *IEEE Commun. Mag.*, 1986, **24**, (4), pp. 25–38

[2] Xiong, F.: '*Digital modulation techniques*' (Artech House, Norwood, MA, 2006)

[3] Bluetooth, S.I.G.: 'The Bluetooth core specification, v4.2', 2014

[4] Yin, Y., Yan, Y., Wei, C.*, et al.*: 'A low-Power low-Cost GFSK demodulator with a robust frequency offset tolerance', *IEEE Trans. Circuits Syst. II, Express Briefs*, 2014, **61**, (9), pp. 696–700

[5] Xi, Z., Zhu, J., Fu, Y.: 'Low-Complexity detection of binary CPM with small modulation index', *IEEE Commun. Lett.*, 2016, **20**, (1), pp. 57–60

[6] Lampe, L., Schober, R., Jain, M.: 'Noncoherent sequence detection receiver for bluetooth systems', *IEEE J. Sel. Areas Commun.*, 2005, **23**, (9), pp. 1718–1727

[7] Bing Li, B.B.: 'Low complexity noncoherent iterative detector for continuous phase modulation systems', *Radioengineering*, 2014, **23**, (3), pp. 0–0

[8] Svedek, T., Herceg, M., Matic, T.: 'A simple signal shaper for GMSK/GFSK and MSK modulator based on sigma-delta look-up table', *Radioengineering*, 2009, **18**, (2), pp. 230–237

[9] Xia, B., Xin, C., Sheng, W.*, et al.*: 'A GFSK demodulator for low-IF bluetooth receiver', *IEEE J. Solid-State Circuits*, 2003, **38**, (8), pp. 1397–1400

[10] Scholand, T., Jung, P.: 'Bluetooth receiver based on zero-crossing demodulation', *Electron. Lett.*, 2003, **39**, (4), pp. 397–398

[11] Laurent, P.: 'Exact and approximate construction of digital phase modulations by superposition of amplitude modulated pulses (AMP)', *IEEE Trans. Commun.*, 1986, **34**, (2), pp. 150–160

[12] Yang, R.H.H., Lee, M.T., Lee, C.K.*, et al.*: 'A novel class of continuous-phase modulation (CPM) with separable phase property'. 2011 Int. Symp. on Intelligent Signal Processing and Communications Systems (ISPACS), Chiang Mai, Thailand, 2011, pp. 1–6

[13] Kaleh, G.K.: 'Simple coherent receivers for partial response continuous phase modulation', *IEEE J. Sel. Areas Commun.*, 1989, **7**, (9), pp. 1427–1436

[14] Taki, M., Nezafati, M.B.: 'A new method for detection of LDPC coded GMSK modulated signals'. 2006 Int. Conf. on Wireless Communications, Networking and Mobile Computing, Wuhan, China, 2006, pp. 1–5

[15] Nelson, T., Perrins, E., Rice, M.: 'Near optimal common detection techniques for shaped offset QPSK and feher's QPSK', *IEEE Trans. Commun.*, 2008, **56**, (5), pp. 724–735

[16] Brown, C., Vigneron, P.J.: 'Complexity reduction for continuous phase modulation using basis functions'. 2009 IEEE Military Communications Conf., Boston, MA, USA, 2009, pp. 1–7

[17] Liang, J.W., Ng, B.C., Chen, J.T.*, et al.*: 'GMSK linearization and structured channel estimate for GSM signals'. Military Communications Conf. (MILCOM'97), vol. **2**, Monterey, CA, 1997, pp. 817–821

[18] Simon, M.K.: '*Bandwidth-efficient digital modulation with application to deep-space communications*' (John Wiley & Sons, Pasadena, CA, USA, 2005)

[19] Laster, J.D.: 'Robust GMSK demodulation using demodulator diversity and BER estimation'. PhD Thesis, Virginia Polytechnic Institue and State University, 1997

[20] Ben Israel, T.N.E.G., Greville Adi, Thomas N. E.: '*Generalized inverses: theory and applications*' (Springer-Verlag, New York, LLC, 2004, 2nd edn.)

[21] Byrd, R.H., Gilbert, J.C., Nocedal, J.: 'A trust region method based on interior point techniques for nonlinear programming', *Math. Program.*, 2000, **89**, (1), pp. 149–185

[22] Heydon, R.: '*Bluetooth low energy: the developer's handbook*' (Prentice-Hall, 2012)